

PENETRATIVE CONVECTION IN A PARTIALLY OPEN ENCLOSURE

Abdulkarim H. Abib and Yogesh Jaluria
Department of Mechanical and Aerospace Engineering
Rutgers, State University of New Jersey
New Brunswick, New Jersey

Abstract

The penetrative convection induced by a localized heat source at the bottom of a partially open enclosure, while the background ambient medium is stably and thermally stratified, is considered. A rectangular cavity with a partially open side is assumed to be adjacent to a long corridor which is stably stratified. The stable thermal stratification that is of interest is a two-layered one or a linear temperature stratification. A control-volume finite-difference method, in stream function and vorticity formulation, is employed for the solution.

The influence of the stratification parameter is examined in the laminar flow regime by considering a range of stratification levels. Heat transfer results, mass outflow rate, penetration distance, velocity and temperature distributions are presented to quantify the penetrative convection.

It is found that, for a step ambient temperature profile, the convective motion occurring in the lower unstable layer penetrates significantly into the stable upper layer only for a weak stratification. Small penetration occurs at large stratification levels. The flow field reveals a multi-cellular pattern. Furthermore, it is observed that the penetrative motion occurs in the form of nearly horizontal motion in the lowest part of the stable upper-layer. The thermal field is studied in detail. Other important details on this penetrative transport are brought out.

NOMENCLATURE

A aspect ratio, $A = L/H$
 g magnitude of the gravitational acceleration, $[m/sec^2]$
 Gr Grashof number based on the height of the cavity
 $Gr = g\beta \frac{Q_0}{\kappa} H^3 / \nu^2$
 H height of the cavity in $[m]$

h_d height of the doorway soffit, $h_d = H_d/H$
 h_w height of the window-sill, $h_w = H_w/H$
 h_0 height of the opening, $h_0 = h_d - h_w$
 L length of the cavity in $[m]$
 l_c length of the corridor, $l_c = L_c/H$
 l_t length of the doorway soffit, $l_t = L_t/H$
 l_s length of the heat source, $l_s = L_s/H$
 $\frac{\dot{m}}{Nu}$ dimensionless mass outflow rate at opening
average Nusselt number over the heat source surface defined in Eq.(20)
 Pr Prandtl number, $Pr = \frac{\mu}{\alpha}$
 Q_0 Total heat input in $[w]$
 \dot{q}''' heat generation per unit volume, $[w/m^3]$
 S stratification Parameter, $S = \Delta T_i / \Delta T_q$
 t dimensionless time
 Δt dimensionless time step
 T temperature in $[^\circ K]$
 ΔT_q characteristic temperature difference, $\Delta T_q = Q_0 / \kappa$ in $[^\circ K]$
 ΔT_i ambient temperature rise in $[^\circ K]$
 u, v dimensionless velocity components in the x and y axes
 X, Y horizontal and vertical coordinates
 z, y dimensionless horizontal and vertical coordinates, $X/H, Y/H$
 z_s dimensionless distance between heat source and the back wall, $z_s = X_s/H$
Greek
 α thermal diffusivity, $[m^2/sec]$
 β coefficient of thermal expansion, $\beta = \frac{1}{T}$ for perfect gas, $[^\circ K^{-1}]$
 ρ density, $[kg/m^3]$
 γ dimensionless ambient temperature gradient defined in Eq.(6)
 κ coefficient of thermal conductivity in $[w/mK]$
 δ_p dimensionless penetration height of the thermal plume

φ	dimensionless temperature, $\varphi = \frac{T-T_{\infty,0}}{\Delta T_q}$
ν	kinematic viscosity in $[m^2/sec]$
Θ	dimensionless temperature, $\Theta = \frac{T-T_{\infty,y}}{\Delta T_q}$
ψ	dimensionless stream function
ζ	dimensionless vorticity

Subscripts

max	maximum value
s	reference to the heat source
w	reference to wall value
∞, y	ambient value at a vertical location y
∞, o	ambient value at the lower-layer ($y = 0$) in two-layer system
∞, u	ambient value at the upper-layer in a two-layer system

INTRODUCTION

Penetrative convection is defined as the process whereby convective motion arising in a stable region penetrates into an adjacent fluid layer which is stably stratified (Turner 1973). The study of penetrative convection is of importance in a wide variety of flows in the environment and in engineering applications. Some common geophysical and engineering examples include:

- The growth of a turbulent atmospheric boundary layer during early morning heating in the absence of wind.
- The deepening of the upper-ocean mixed layer into the stably stratified pycnocline owing to the turbulence induced by surface wind or cooling.
- The mixing at the thermocline due to the discharge of a buoyant jet from a power plant heat rejection system.
- The terminal or penetration height of a buoyancy-induced rise of smoke and other combustion products in an enclosure fire due to the presence of stable, thermal stratification in the ambient medium.

In view of the present-day environmental problems, such mixing processes are important in the study and control of various biological activities (in water bodies such as ocean and lakes), in the dispersion of pollutants in the environment, and the prediction of movement of smoke in the buildings. For instance, the dispersal of pollutants released into the atmosphere will depend on the rate of growth of the atmospheric boundary layer in the lower part of the atmosphere. Similarly, penetrative convection in a cooling pond will affect the heat from the warm inflow and, hence, the power plant intake and efficiency. In enclosure fires, the mixing caused by the penetrative convection will affect the height of the hot-cold interface between the hot combustion products and lower region containing the inflow of cold air. This will, in turn, influence the fire-fighting and rescue operations, as well as the fire detection, control and extraction systems for smoke and other toxic gases (McCaffrey & Quintiere 1977).

A considerable amount of work has been done over the past three decades on external flows such as plumes and boundary layers in the presence of a stable, thermal ambient stratification. The results have been summarized by Turner (1973), Jaluria (1980), and List (1982). On the other hand, results for cavity flows with stratification are much less extensive, but include the

studies of Walin (1971), Chen et al. (1971), and Torrance (1979).

Various experimental and numerical studies of penetrative convection have been reported in which a stable layer in a tank with an initially linear or two-layer ambient temperature stratification is eroded from below by unstable mixed layer generated by heating the bottom (Deardorff et al. 1969; Kato & Phillips 1969; Willis and Deardorff 1974; Denton & Wood 1981; Heidt 1977; and Kumar 1989). In all these cases there is no mean flow and hence no shear present. Svensson (1978), Zeman & Lumley (1976) and Mellor & Yamada (1982) reported numerical simulation of a similar experiment carried out by Willis & Deardorff (1974) using a number of different turbulent models. For more details, see the recent review by Rodi (1987).

Penetrative convection is also produced by cooling water below its maximum density temperature of 4°C at the base of a water column. In this case, it leads to steady state penetrative convection. This problem was studied experimentally by Townsend (1964) and later solved numerically by Musman (1968).

The penetrative convection of wall flows, such as buoyancy-induced or ceiling-jet driven wall flows, are very important at various stages of fire growth, and at several locations, these flows are subject to an opposing buoyancy force. These flows are called negatively buoyant and have been investigated by many researchers. See the recent review by Jaluria & Cooper (1989).

The results for vented or partially open cavities and their interaction with stratified ambient medium are essentially non-existent. Therefore, in present study, penetrative convection in a partially open enclosure with a localized heat source at bottom boundary is considered. Only laminar flows are examined here. The turbulent flow study is reported by Abib (1992).

MATHEMATICAL FORMULATION

The Problem

Penetrative convection in an enclosure, where the background ambient medium is stably and thermally stratified, is considered. A 2-D rectangular cavity with a partially open side is examined. The aspect ratio A is held constant at a value of 2 which is a typical of room-size enclosures. The cavity or room (see Fig. 1) is adjacent to a long corridor of 4 times the height of the cavity. The corridor is stably stratified, for instance, due to some earlier fire activity. The stable thermal stratification, that is of interest in the present study, is a two-layered or a linear temperature stratification heated from below by a small localized heat source, which may represent a fire.

Governing Equations

The governing equations, in dimensionless form, expressing conservation of mass, momentum, and energy, for incompressible Boussinesq fluid, can be written as:

$$u = \frac{\partial \psi}{\partial y}; \quad v = -\frac{\partial \psi}{\partial x} \quad (1)$$

$$\frac{\partial^2 \psi}{\partial x^2} + \frac{\partial^2 \psi}{\partial y^2} = -\zeta \quad (2)$$

$$\frac{\partial \zeta}{\partial t} + \frac{\partial(u\zeta)}{\partial x} + \frac{\partial(v\zeta)}{\partial y} = \frac{1}{\sqrt{Gr}} \left\{ \frac{\partial}{\partial x} \left(\frac{\partial \zeta}{\partial x} \right) + \frac{\partial}{\partial y} \left(\frac{\partial \zeta}{\partial y} \right) \right\} + \frac{\partial \Theta}{\partial x} \quad (3)$$

$$\frac{\partial \Theta}{\partial t} + \frac{\partial(u\Theta)}{\partial x} + \frac{\partial(v\Theta)}{\partial y} + v\gamma = \frac{1}{Pr\sqrt{Gr}} \left\{ \frac{\partial}{\partial x} \left(\frac{\partial \Theta}{\partial x} \right) + \frac{\partial}{\partial y} \left(\frac{\partial \Theta}{\partial y} \right) \right\} + \frac{1}{Pr\sqrt{Gr}} \left\{ \dot{q}''' + \frac{d^2 \Theta_{\infty,y}}{dy^2} \right\}. \quad (4)$$

When considering the two-layer ambient temperature, a sharp interface is physically not reasonable and the temperature jump at the interface is approximated by a gradual rise, using the following expression

$$T_{\infty,y} = 0.5 \Delta T_i \left\{ 1 + \tanh \left[b \left(\frac{Y}{H} - \frac{H_i}{H} \right) \right] \right\} \quad (5)$$

where ΔT_i is the temperature jump at the interface, H_i is the height of the interface and b is specified constant. By choosing b equal to either 10 or 20, we can approximate the ambient temperature profile satisfactorily. Due to smoothing of the step profile, an interfacial layer is created with a width given as $\Delta H_i = 2Hb^{-1}$. The smaller the interfacial layer gets the better the approximation of the step profile becomes.

The dimensionless ambient temperature gradient γ is given by

$$\gamma = \frac{H}{\Delta T_q} \frac{dT_{\infty,y}}{dY} = 0.5b \frac{\Delta T_i}{\Delta T_q} \operatorname{sech}^2 \left[b \left(\frac{Y}{H} - \frac{H_i}{H} \right) \right]. \quad (6)$$

The ratio $S = \Delta T_i / \Delta T_q$ that appears in the expression of the ambient temperature gradient γ is called the stratification parameter. The stratification parameter S can also be considered as the dimensionless temperature rise at the interface. Since the dimensionless temperature Θ is defined relative to the ambient temperature $T_{\infty,y}$ an extra term $v\gamma$ appears in the energy Eq.(4). This term describes the vertical convection in a stratified medium. In an isothermal ambient case, $T_{\infty,y}$ is constant and the extra term becomes zero.

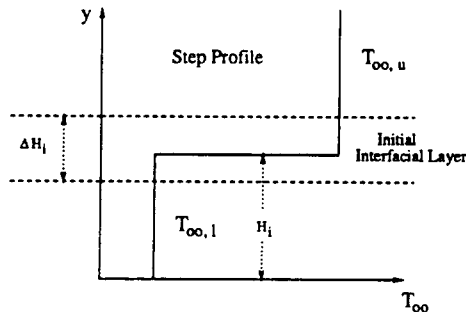
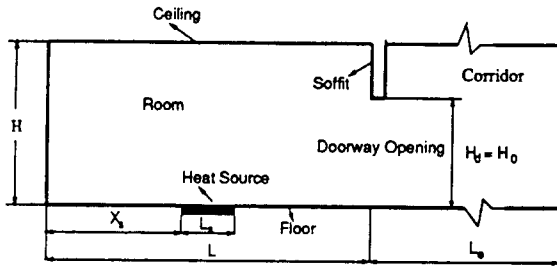


Figure 1: Room and corridor regions with a step ambient temperature stratification.

Using H , ΔT_q , and $H/\sqrt{g\beta\Delta T_q H}$ as reference length, temperature, and time scales, the governing equations introduce three dimensionless parameters: the Grashof number, the Prandtl number, and the stratification parameter, defined as

$$Gr = \frac{g\beta\Delta T_q H^3}{\nu^2}, \quad Pr = \frac{\nu}{\alpha}, \quad S = \frac{\Delta T_i}{\Delta T_q}. \quad (7)$$

Since fluid considered is air the Prandtl number Pr is set to a value of 0.72. The aspect ratio A is generally held constant at a value of 2 (typical of room fires). The size of the heat source is also fixed ($L_s = 0.2H$). The location of the heat source is taken as the middle of the bottom surface ($X_s = 0.9H$). The location of the stable layer interface is also fixed ($H_i = 0.5H$) for the calculations. Other values besides these typical values were also considered. But the basic trends obtained were found to be the same as those at these typical values.

Initial and Boundary Conditions

The initial and boundary conditions for the governing equations (2) - (4) are specified as

- Initial condition at $t < 0$:

$$u = v = \psi = \zeta = \Theta = 0, \quad 0 \leq x \leq x_{max} \text{ and } 0 \leq y \leq 1 \quad (8)$$

- Boundary conditions at $t \geq 0$:

1. Bottom boundary (floor) at $y = 0$:

$$u = v = \psi = 0, \quad \zeta = \zeta_w, \quad 0 \leq x \leq x_{max} \quad (9)$$

$$\frac{\partial \Theta}{\partial y} = \begin{cases} 0 & 0 \leq x \leq x_s \\ \dot{q}'' = \frac{1}{l_s} & x_s \leq x \leq x_s + l_s \\ 0 & x_s + l_s \leq x \leq x_{max} \end{cases} \quad (10)$$

2. Ceiling at $y = 1$ and doorway soffit at $y = h_d$:

$$u = v = \psi = \frac{\partial \Theta}{\partial y} = 0, \quad \zeta = \zeta_w, \quad 0 \leq x \leq x_{max} \quad (11)$$

3. Left side wall or back wall at $x = 0$:

$$u = v = \psi = \frac{\partial \Theta}{\partial x} = 0, \quad \zeta = \zeta_w, \quad 0 \leq y \leq 1 \quad (12)$$

4. Door soffit walls at $x = A$ and $x = A + l_c$:

$$u = v = \psi = 0, \quad \zeta = \zeta_w, \quad \frac{\partial \Theta}{\partial x} = 0, \quad h_d \leq y \leq 1 \quad (13)$$

5. Right far-field boundary at $x = x_{max}$:

$$v = \frac{\partial u}{\partial x} = \frac{\partial \psi}{\partial x} = \frac{\partial \zeta}{\partial x} = 0, \quad 0 \leq y \leq 1 \quad (14)$$

$$\begin{cases} \Theta = 0 & \text{if } u \leq 0 & (\text{inflow}) \\ \frac{\partial \Theta}{\partial x} = 0 & \text{if } u > 0 & (\text{outflow}) \end{cases} \quad (15)$$

For the wall vorticity ζ_w , a first-order form is used

$$\zeta_w = -2 \frac{\psi_{w+1} - \psi_w}{\Delta n^2} + O(\Delta n) \quad (16)$$

where n is the direction normal to wall. This first-order form is the safest form to use and often gives results essentially equal to the higher-order forms (Roache, 1972).

NUMERICAL SOLUTION

The governing equations are discretized with the control-volume finite-difference method (see Abib, 1992 for details). The solution of Θ , ζ , and ψ are obtained by an iterative procedure at each time step. The iterative method is a double loop in which the inner loop is a line by line method, in which tridiagonal matrix is inverted in each sweep direction, for the variables Θ and ζ and a SOR for ψ .

The existence of the boundary layer near the walls requires that a non-uniform grid to be used that gives a strong grid refinement along the walls. We used a hyperbolic grid distribution defined as

$$\frac{X_i}{H} = \frac{1}{2} \left\{ 1 + \frac{\tanh[\alpha_1(i/i_{max} - \frac{1}{2})]}{\tanh(\alpha_1/2)} \right\} \quad i = 0, 1, 2, \dots, i_{max} \quad (17)$$

$$\frac{Y_i}{H} = \frac{1}{2} \left\{ 1 + \frac{\tanh[\alpha_1(i/i_{max} - \frac{1}{2})]}{\tanh(\alpha_1/2)} \right\} \quad i = 0, 1, 2, \dots, i_{max} \quad (18)$$

where α_2 is given by $\alpha_2 = \alpha_1 / \sinh(\alpha_1)$. In all the calculations we took $\alpha_2 = 1.5 \times 10^{-3}$ which gives $\alpha_1 = 6.811$ to ensure that at least 8 to 10 points lie between the wall and the location of maximum velocity. In the y-direction, extra grid points are added at the location of the interface of a step ambient temperature profile in order to resolve sharp gradients. Also, in the x-direction, extra points (10 points) are added near the location of the heat source.

Using the analogy of buoyancy-driven flows in a cavity with differentially heated side walls (see Gills 1966, Patterson & Imberger 1980, and Henkes 1990), the time evolution in the open cavity at large Gr is dominated by two time scales:

$$t_1 = \frac{A^2 H^2}{\nu} (GrPr)^{-1/4} \quad t_2 = \frac{H^2}{\nu} (GrPr)^{-1/2} \quad (19)$$

The diffusion time scale $t_0 = \frac{H^2}{\nu} (GrPr)^0$ is the dominant time scale at small Gr , but is of minor importance at large Gr . The time scale t_1 is larger than t_2 and determines the needed time to reach the steady state. The time scale t_2 is the Brunt-Vaisala time scale and determines the maximum time step that still gives a stable numerical solution. This time step limitation has also been reported by Jones (1985), Thompson et al. (1987), and Henkes (1990) from their study of buoyancy-driven turbulent flow in a rectangular cavity. The required number of time steps is estimated as $t_{max} = \frac{t_1}{t_2} = A^2 (GrPr)^{1/4}$. For all cases, a time step $\Delta t = \frac{1}{10}$ or $\frac{1}{5}$ is used to ensure a stable numerical solution.

RESULTS AND DISCUSSION

For the present study, the following parameters are held fixed.

- $h_0 = 0.8$ (the height of the doorway opening).
- $h_i = 0.5$ (initial location of the interface).

The governing parameters of the problem are the Grashof number Gr and the stratification parameter $S = \Delta T_i / \Delta T_q$. In the present work, the influence of stratification parameter is explored for moderate Gr ($Gr = 2 \times 10^7$ and 2×10^8 , laminar flow cases). The stratification parameter S is varied in the range from 0 to 1 for the given range of Gr . A value of S larger than 1 means that the ambient temperature rise is larger than the driving temperature difference $\Delta T_q = Q_0 / \kappa$. These extreme cases

of initial stratification of the ambient medium have no practical interest. For a given Gr , say $Gr = 2 \times 10^8$, $S < 0.1$ is a relatively weak stratification, while $S \geq 0.1$ is a stronger stratification. A steady state solution is sought, when one exists, by solving numerically the initial-value problem. The computed results are discussed in the following section.

Transient Behavior

The numerical solution of the initial-value problem is carried out by marching in time until a steady state is reached. The achievement of a true steady state is made difficult by the presence of the internal gravity waves for values of $Gr \geq 2 \times 10^8$. For instance, at $Gr = 2 \times 10^7$ and lower, a steady state is reached after the oscillations are damped, as can be seen in the plots of Θ_1 against time in Fig. 2. At $Gr = 2 \times 10^8$, for values of $S > 0$, oscillations developed. These oscillations are shown in Fig. 3 for the temperature Θ_1 at one of the monitoring points in cavity ($x=0.036$, $y=0.5$) near the left wall for different values of the stratification parameter S . The oscillations become more pronounced as S is increased. This is indicated in Fig. 3. The amplitude of the temperature oscillations is very small, in fact, as small as 4×10^{-4} which is about 1.0% of the mean value of Θ_1 . However its presence is not desired and results in a tremendous increase in computer time since it becomes necessary to run the computer program for a long time to reach the steady state or periodic solutions.

It was not clear, at the beginning, if these oscillations were numerical or physical. They could be physical because of internal gravity waves, particularly when the medium is stratified.

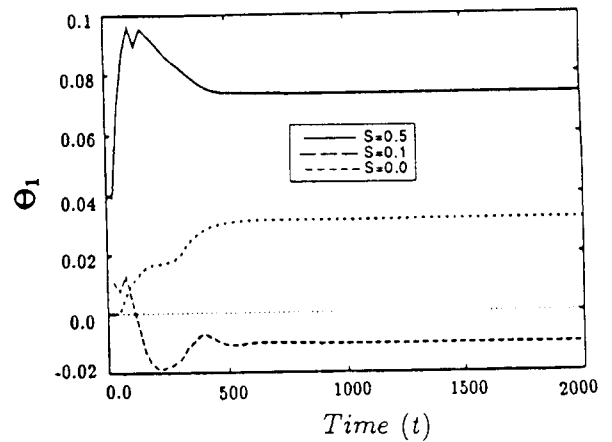


Figure 2: The temporal development of the temperature Θ_1 at a given location ($x = 0.036$, $y = 0.5$), at $Gr = 2 \times 10^7$, and with various step ambient temperature stratifications.

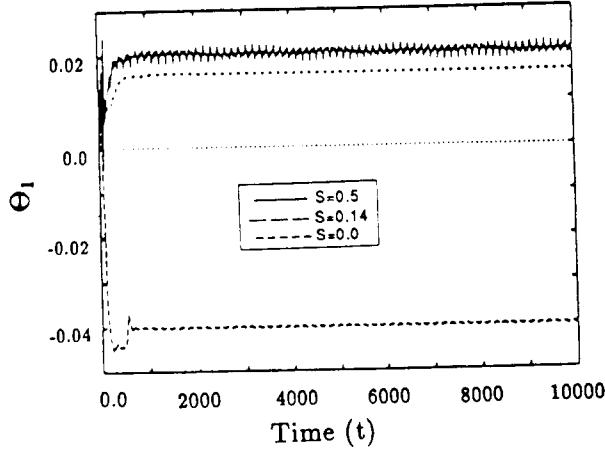


Figure 3: The temporal development of the temperature Θ_1 at a given location ($x = 0.036$, $y = 0.5$), at $Gr = 2 \times 10^8$, and with various step ambient temperature stratifications.

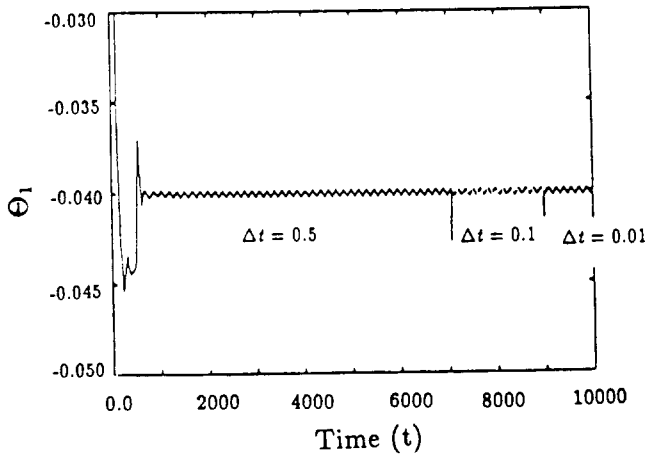


Figure 4: The effect of time step on the temporal evolution of the temperature Θ_1 for a step ambient temperature stratification ($S = 0.14$) at a given location $x = 0.036$, $y = 0.5$ inside the cavity and at $Gr = 2 \times 10^8$.

Therefore, calculations were performed with a refined grid. A sequence of non-uniform grids of 53×55 points (with 30×30 grid points inside the cavity) and 83×85 points (with 60×60 grid points inside the cavity) have been used to ensure the grid independence of computed oscillations. When oscillations are obtained, it is necessary to reduce the time step to check whether the oscillations still exist or not. Time steps of 0.5, 0.1, and 0.01 were used. In fact, starting from the initial condition of quiescent and thermal stratification (say $S=0.14$), Θ_1 evolve in an oscillatory fashion. By reducing the time step and re-calculating, using the previous result as the initial approximation, the periodic nature (constant amplitude) of the oscillation becomes apparent. This is shown in Fig. 4.

Influence of Stratification parameter

Increasing S , while holding Gr fixed, may be interpreted as increasing the stratification temperature difference or the interface temperature jump or rise ΔT_i while holding the natural convection driving force $\Delta T_q = \dot{Q}_0/\kappa$ fixed (Torrance, 1979). Many experimental runs, with different Gr in the range of 2×10^6 to 2×10^8 , are made to explore the effect of stratification. In each case with a fixed Gr , the stratification parameter S is varied from $S = 0.01$ to $S = 0.5$. For the sake of conciseness, the case with $Gr = 2 \times 10^8$ is presented and discussed in detail to determine the influence of thermal stratification. Both step and linear ambient temperature profiles are examined. But, due to lack of space the results for the step ambient temperature case are presented. Furthermore, only the two extreme cases of ambient stratification are reported. These are $S = 0.5$ corresponding to a strong ambient stratification and $S = 0.05$ corresponding to a relatively weak ambient stratification. See Abib (1992) for further detail.

Flow and Thermal Fields. Figure 5 shows the variation of the steady state temperature and stream function with the stratification parameter S for a step ambient temperature distribution at $Gr = 2 \times 10^8$. In Fig. 5, individual graphs from (a) to (b) pertain to a variation in S as $S = 0.05$ and 0.5 . In each graph, the isotherms are plotted at the top frame and the stream function at the bottom frame. In the plots, the stream function ψ is scaled by \sqrt{Gr} and the temperature Θ by $Gr \times 10^{-6}$.

The flow field reveals a multi-cellular pattern. This can be seen in the bottom frame in Fig. 5(a) and (b). There is one main or primary cell and a counter cell above it. The largest velocities are found in the main convective cell which extends from the lower boundary (floor) to the location where the wall plume reaches a stagnation point and then turns horizontally toward the opening. The height of the location of the stagnation point is defined here as the penetration height δ_p . The horizontal motion at the top of the main cell is towards the right, in the direction of the opening doorway, while the motion at the bottom of the main cell is towards the left, in the direction of the back wall. For the counter cell, it is the other way around. The flow in the main cell is caused by buoyancy of the fluid inside the cavity which is warmer than the surrounding fluid outside the opening. In the upper part of the cavity, the temperature level is lower than that of the ambient medium at the same height. A counter-rotating cell is generated by the pressure difference due to the expansion of gases or fluid produced by the temperature difference between

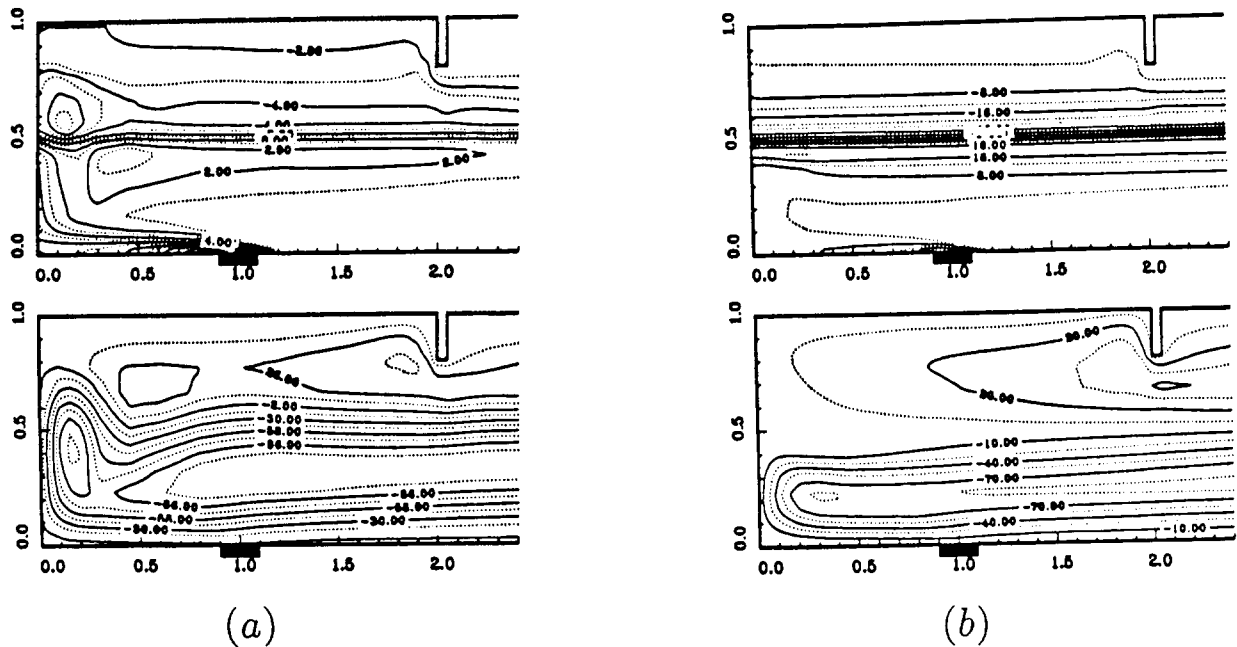


Figure 5: Isotherms and streamlines at $Gr = 2 \times 10^8$ with step ambient temperature stratifications. (a) $S = 0.05$ and (b) $S = 0.5$.

the upper region of the cavity and the ambient medium. The circulation and the velocities in the counter cell are substantially less than those of the main cell.

The convective motions occurring in the lower unstable region may penetrate into the upper stable region for a weaker stratification ($S \leq 0.1$, at $Gr = 2 \times 10^8$). The penetration of convective motion takes place in the form of nearly horizontal flow in the bottom part of the stable layer, corresponding to the top part of the main cell, as indicated by the stream lines in Fig. 5. A behavior similar to this has also been reported by Musman (1968), in his study of penetrative convection which depended on the density maximum of water near 4°C . Here, $S = 0.5$ corresponds to a strong ambient stratification and the penetration height of the main cell is obtained as $\delta_p = 0.37$ in a step ambient temperature case. A decrease in S intensifies the thermal plume and the amount of circulation in the main cell and, hence, increases the penetration height. For $S = 0.05$ or smaller, the plume hits the ceiling and a ceiling jet forms. See the review by Quintiere (1984) and Jaluria & Cooper (1989) for cases with behavior similar to this. In the absence of stratification $S = 0$, a natural convection flow driven by the heat source is obtained. The results for such flows are given by Abib (1992).

The isotherms plotted in the top frames of Fig. 5(a) and (b) display the influence of S on the plume development near the heat source. At smaller values of S , the thermal plume is well established near the heat source and is able to penetrate into the upper layer. However, at large values of S , the plume is confined to the lower-layer since it is unable to penetrate into the hot upper-layer. This is expected physically since the thermal stratification of the medium would affect the plume rise by

lowering the temperature difference between the fluid element and the ambient medium and, hence, the buoyancy force. Both positive and negative temperature values appear in the contour plot. At a fixed height, positive temperature values indicate that the fluid element is hotter than the ambient medium at that particular height, whereas, negative temperature values mean that the fluid is colder than the ambient at the same height.

Temperature and Velocity Profiles. The vertical distribution of the computed temperature φ and the horizontal component of the velocity u at three horizontal locations, namely $x = 0.5, 1.0$, and 2.0 , for step ambient temperature stratifications, are plotted in Figs. 6 and 7. The figures illustrate the influence of S at $Gr = 2 \times 10^8$.

The vertical variation of the temperature at different horizontal locations, in Fig. 6, look similar, in particular, away from the walls and from the heat source. This means that the horizontal temperature gradients are small except in the thermal plume above the source. Three distinct regions can be identified for the vertical temperature profiles. These are the lower-layer which is at a quasi-uniform temperature; the stratified layer between the lower and upper layers; and the upper-layer which is also at a uniform temperature either at or lower than the ambient temperature.

The vertical distribution of the horizontal component of the velocity u is shown in Fig. 7 for different S values. The u -velocity profiles show a strong convective main cell and a weaker counter cell above it. In the main cell, there is inflow of cooler fluid at the bottom of the cell and outflow of warmer fluid at the top part of the cell. The various curves collapse into an almost single

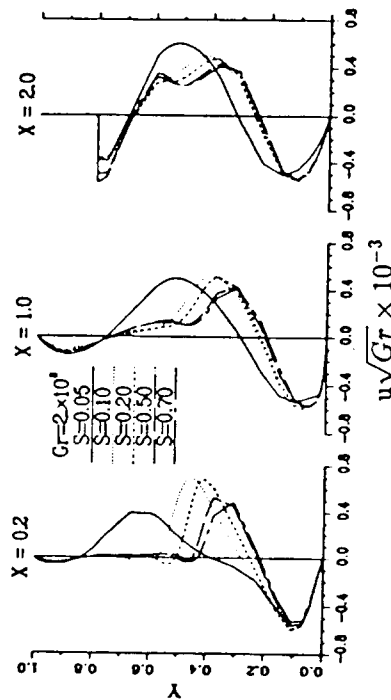


Figure 7: The vertical distribution of the horizontal component of the velocity u , at $Gr = 2 \times 10^8$ with various step ambient temperature stratifications.

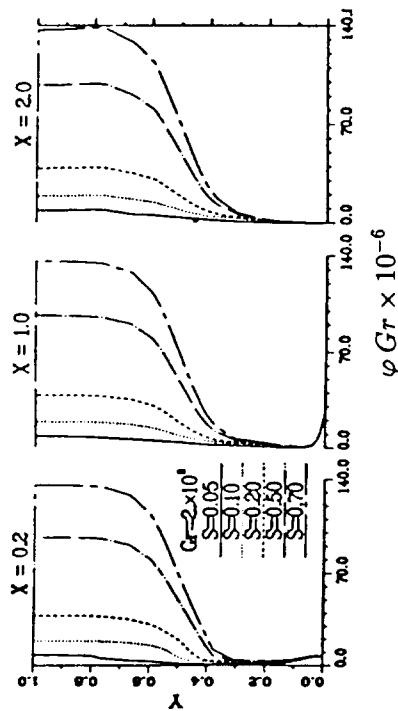


Figure 6: The vertical distribution of the temperature $\varphi = \frac{T - T_{\infty,0}}{Q_0/\kappa}$, at $Gr = 2 \times 10^8$ with various step ambient temperature stratifications.

curve at the bottom, while at the top of the main cell the effect of S is more pronounced. This is physically expected because at bottom of the main cell (in the lower layer), the ambient temperature gradient is zero, whereas at the top of the cell, in the vicinity of the interface, the ambient temperature gradient is large and, hence, the effect of S is more pronounced. The result is the lowering of the maximum horizontal velocity u_{max} as S increases. The vertical location of the u_{max} is also shifted towards the bottom surface as S increases. Note that penetration takes place in the form of horizontal motion at the top part of the main cell. Therefore, the penetration distance is computed as the maximum vertical location where the horizontal component of the velocity u in the top part of the main cell becomes zero. In other studies such as, for instance that of Goldman & Jaluria (1986) and Kapoor & Jaluria (1992), the penetration distance is obtained by plotting the vertical temperature distribution and taking a sharp change in the profiles as indication of the extent of the penetration of the wall jet. The penetration distance obtained in the same criteria as that of Goldman & Jaluria involves a large margin of (20-30%) in error. This is because, as can be seen in the temperature profiles, there is no sharply defined change in the temperature profiles due to the presence of stratified layer in between the lower and the upper isothermal layers.

Penetration Distance. The penetration distance δ_p is plotted against the stratification parameter S in Fig. 8 for both step and linear ambient temperature profiles. The graph shows that, as the stratification parameter S is increased, the penetration distance decreases rapidly, for small values of S ($0 <$

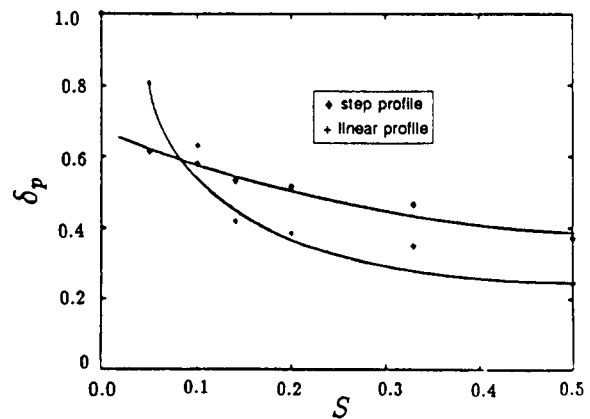


Figure 8: Penetration distance δ_p versus the stratification parameter S , at $Gr = 2 \times 10^8$. The symbols are the results from numerical solutions. The lines are obtained by least squares curve fitting.

$S < 0.2$). It then slowly and almost linearly decreases for higher value of S that correspond to stronger stratification. At $S > 0.3$, the main cell is unable to penetrate into the stable upper layer. This is indicated by the fact that the corresponding δ_p is less than 0.45 (the location of the interfacial layer). One would expect that as S is increased beyond 0.5, the penetration distance to remain constant (for step profile) since the flow cannot penetrate into the upper stable layer. This does not happen because the increased stratification would not only decrease the buoyancy level of the main cell but it will also act as a source of energy. As a result, a counter cell is created above the main cell. This counter cell may grow in size and therefore the main cell has to adjust accordingly. Consequently the penetration distance of the main cell is lowered. In the case of the linear profile, this drop is more vigorous because the buoyancy is lowered even more due to the increasing ambient temperature with height.

Heat Transfer and Mass Outflow Rates. The influence of the stratification parameter S on the heat transfer and mass outflow rates is considered here. The average heat transfer rate at the source is given by the average Nusselt number based on the height of the cavity as

$$\overline{Nu} = \frac{\bar{h}H}{\kappa} = \frac{1}{l_s^2} \int_0^{l_s} \frac{1}{\Theta_s} dx \quad (20)$$

Here l_s is dimensionless length of the source, $l_s = L_s/H$, and Θ_s is the dimensionless temperature at the surface of the source. H is the height of the cavity and it is here taken as the characteristic length scale because it determines the size of the largest eddies in the vertical direction.

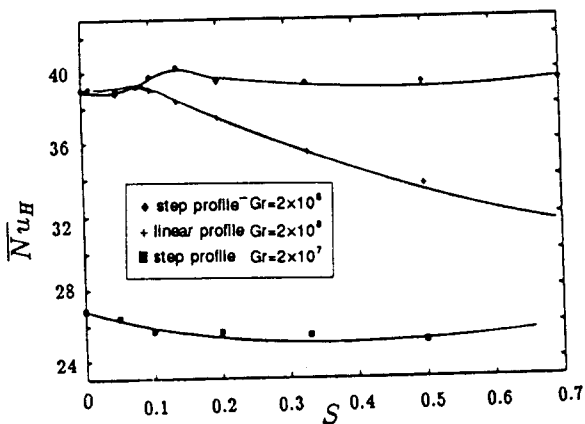


Figure 9: Average Nusselt number \overline{Nu} versus the stratification parameter S at $Gr = 2 \times 10^8$. The symbols are the results from numerical solutions. The lines are obtained by least squares curve fitting.

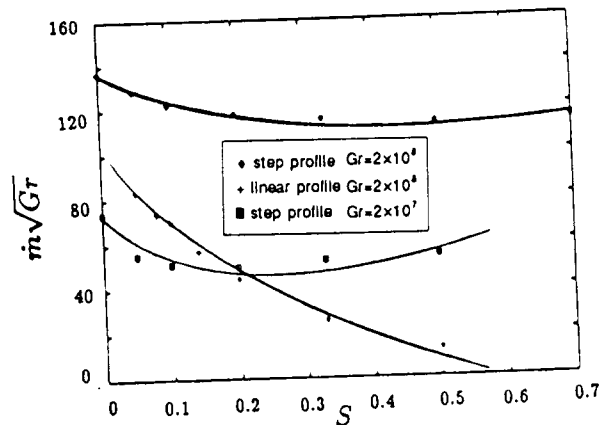


Figure 10: Average mass outflow rate \bar{m} versus the stratification parameter S at $Gr = 2 \times 10^8$. The symbols are the results from numerical solutions. The lines are obtained by curve least squares fitting.

The effect of S on \overline{Nu} is shown in Fig. 9 for step (\circ) and linear ($+$) ambient temperature profiles. The solid and broken lines curves in Fig. 9 are obtained by least squares curve fitting. The figure shows that, in a linear profile, as S is increased the Nusselt number decreases slowly at the lower value of S and then at a higher rate for large values of S . On the contrary, the Nusselt number does not vary much in the case of the step profile. The variation is less than 2.5-3.0%. This is because, in a linear profile, the ambient temperature varies with height and, therefore, stratification lowers the temperature difference between the source and the ambient medium. The result is lower velocities, smaller mass flow rate and lower heat transfer. In the step profile, the ambient temperature varies with height only in the vicinity of the interface. The main convective cell which is responsible for most of the flow and the thermal pattern is confined to the lower-layer where the ambient temperature gradient is zero. Therefore, the effect of S on the heat transfer and the flow rates is small.

Figure 10 shows the mass outflow rate at the opening versus S for step (\circ) and the linear ($+$) ambient temperature profiles. The mass outflow rate decreases with an increase of S in both cases. This is physically expected because stratification can be viewed as an impediment to the flow in the sense that the stratification reduces the buoyancy level and, hence, results in lower velocities and smaller mass flow rates.

CONCLUSION

A penetrative convection, in a partially open enclosure heated from below by a localized energy source and with stably strat-

ified ambient medium, has been studied. The study mainly focussed attention on the interaction between the open cavity and the environment factors such as temperature stratification of the ambient medium for moderate Gr.

In the range of the stratification parameter S examined, it was found that for small values of S the thermal plume reaches the ceiling, while for large values of S it is unable to penetrate into the stable upper-layer. The flow exhibits a multi-cellular pattern consisting of a main convective cell at the bottom part of the cavity and a weak counter cell at the top. The penetrative flow takes places in the form of horizontal motion in the lowest part of the stable upper-layer which corresponds to the top part of the main cell.

The thermal stratification reduces the buoyancy level and, hence, results in lower velocities, smaller mass flow rate, lower heat transfer rate, and lower penetration distance.

ACKNOWLEDGMENTS

The authors acknowledge the partial support provided by the Building and Fire Research Laboratory, National Institute of Standards and Technology, under Grant No. 60NANB7D0743 for this work.

REFERENCES

- Abib, A.H., 1992, "Penetrative and Recirculating Flows in Enclosures with Openings", *Ph.D. Thesis*, Rutgers University, New Brunswick, NJ.
- Chen, C.F., Briggs, D.B. and Wirtz, R.A., 1971, "Stability of Thermal Convection in a Salinity Gradient Due to Lateral Heating", *Int. J. Heat Mass Transfer*, Vol. 14, pp. 57.
- Denton, R.A. and Wood, I.R., 1981, "Penetrative Convection at Low Peclet Number", *J. Fluid Mech.*, Vol. 113, pp. 1-21.
- Deardorff, J.W., Willis, G.E., and Lilly, D.K., 1969, "Laboratory Investigation of Non-steady Penetrative Convection", *J. Fluid Mech.*, Vol. 35, pp. 7-31.
- Heidt, F.D., 1977, "The Growth of a Mixed Layer in a Stratified Fluid", *Boundary Layer met.*, Vol. 12, pp. 439-461.
- Gill, A.E., 1966, "The Boundary Layer Regime for Convection in a Rectangular Cavity", *J. Fluid Mech.*, Vol. 26, pp. 515-536.
- Goldman, D. and Jaluria, Y., 1986, "Effect of Opposing Buoyancy on the Flow in Free and Wall Jet", *J. Fluid Mech.*, Vol. 166, pp. 41-56.
- Henkes, R.A.W.M., 1990, "Natural Convection Boundary Layers", *Ph.D. Thesis*, Delft University, Delft, The Netherlands.
- Jaluria, Y., 1980, "Natural Convection Heat and Mass Transfer", Pergamon Press, U.K.
- Jaluria, Y. and Cooper, L.Y., 1989, "Negatively Buoyant Wall Flows Generated in Enclosure Fires", *Proc. Energy Combust. Sci.*, Vol. 15, pp. 159-182.
- Jones, I.P., 1985, "The Convergence of a Simple Iterative Strategy for Strongly Stratified Flows", *Numer. Meth. on Laminar and Turbulent Flow*, C. Taylor (Ed.), pp. 733-740, Pineridge Press.
- Kapoor, K. and Jaluria, Y., 1992, "Penetrative Convection of a Plane Turbulent Wall Jet in a Two-layer Thermally Stratified Environment", to appear in *Int. J. Heat Mass Transfer*.
- Kato, H. and Phillips, O.M., 1969, "On the Penetration of a Turbulent Layer into a Stratified Fluid", *J. Fluid Mech.*, Vol. 37, pp. 643-655.
- Kumar, R., 1989, "Laboratory Studies of Thermal Convection in the Interface under a Stable Layer", *Int. J. Heat Mass Transfer*, Vol. 32, pp. 735-749.
- List, E.J., 1982, "Turbulent Jets and Plumes", *Ann. Rev. Fluid Mech.*, Vol. 14, pp. 189-212.
- Mellor, G.L. and Yamada, T., 1982, "Development of a Turbulence Closure Model for Geophysical Fluid Problems", *Rev. Geophys.*, Vol. 20(4), pp. 851-875.
- McCaffrey, B.J. and Quintiere, J.G., 1977, "Buoyancy Driven Countercurrent Flow Generated by a Fire Source", in Spalding, D.B., and Afgan, N. (Eds.), *Heat Transfer and Turbulent Buoyant Convection*, Vol. II, pp. 457-472, Hemisphere, Washington, D.C.
- Musman, S., 1968, "Penetrative Convection", *J. Fluid Mech.*, Vol. 31, pp. 343-360.
- Patterson, J. and Imberger, J., 1980, "Unsteady Natural Convection in a Rectangular Cavity", *J. Fluid Mech.*, Vol. 100, pp. 65-86.
- Quintiere, J.G., 1984, "Perspective on Compartment Fire Growth", *Combust. Sci. Technol.*, Vol. 39, pp. 11-54.
- Roache, P.J., 1972, "Computational Fluid Dynamics", Hermosa Publishers, Albuquerque, New Mexico.
- Rodi, W., 1987, "Examples of Calculation Methods for Flow and Mixing in Stratified Fluids", *J. Geophys. Res.*, Vol. 92, No. C5, pp. 5305-5328.
- Svensson, U., "Mathematical Model of the Seasonal Thermocline", *Dept. of Water Resour. Eng. Rep. 1001*, Univ. of Lund, Lund, Sweden.
- Thompson, C.P., Wilkes, N.S. and Jones, I.P., 1987, "Numerical Studies of Buoyancy-Driven Turbulent Flow in a Rectangular Cavity", *Int. J. Num. Meth. Engng.*, Vol. 24, pp. 89-99.
- Torrance, K.E., 1979, "Natural Convection in Thermally Stratified Enclosures with Localized Heating from Below", *J. Fluid Mech.*, Vol. 95, pp. 477-495.
- Townsend, A.A., 1964, "Natural Convection in Water over an Ice Surface", *Quarterly J. Roy. Meteor. Soc.*, Vol. 90, pp. 248-259.
- Turner, J.S., 1973, "Buoyancy Effects in Fluids", Cambridge University press, London.
- Walsh, G., 1971, "Contained Non-homogeneous Flow under Gravity or How to Stratify a Fluid in the Laboratory", *J. Fluid Mech.*, Vol. 48, pp. 647.
- Willis, G.E. and Deardorff, J.W., 1974, "A Laboratory Model of the Unstable Planetary Boundary Layer", *J. Atmos. Sci.*, Vol. 31, pp. 1297-1307.
- Zeman, O. and Lumley, J.L., 1976, "Modeling Buoyancy-Driven Mixed Layers", *J. Atmos. Sci.*, Vol. 33, 1974-1988.